BOLETIN LATINOAMERICANO Y DEL CARIBE DE PLANTAS MEDICINALES Y AROMÁTICAS
© / ISSN 0717 7917 / www.blacpma.ms-editions.cl

Articulo Original / Original Article

Identification of cancer inhibitors from *Hystrix brachyura* bezoar extracts using LC-MS multivariate data analysis and in silico evaluation on Bcl-2, cyclin B/CDK1, VEGF and NM23-H1

[Identificación de inhibidores de cáncer a partir de extractos de bezoar de *Hystrix branchyura* usando análisis multivariado LC-MS y evaluación in silico en Bcl-2, cyclin B/CDK1, VEGF, y NM23-H1]

Al' aina Yuhainis Firus Khan[1,2], Qamar Uddin Ahmed[3], Alfi Khatib[3], Zalikha Ibrahim[3], Tanzina Sharmin Nipun[4], Hatim Abdullah Natto[2,5], Mohd Zuwairi Saiman[6,7], Zainul Amiruddin Zakaria[8] & Ridhwan Abdul Wahab[9]

[1]Department of Science Education, Faculty of Education, Universiti Teknologi MARA, Puncak Alam, Malaysia
[2]Department of Biomedical Sciences, Kulliyyah of Allied Health Sciences, International Islamic University Malaysia, Kuantan, Malaysia
[3]Pharmacognosy Research Group, Department of Pharmaceutical Chemistry, Kulliyyah of Pharmacy, International Islamic University Malaysia, Kuantan, Malaysia
[4]Department of Pharmacy, Faculty of Biological Sciences, University of Chittagong, Chittagong, Bangladesh
[5]Department of Epidemiology, College of Public Health and Health Informatics, Umm Al-Qura University, Makkah Al Mukaramah, Saudi Arabia

(Continue before References)

Reviewed by:
Ali Parlar
Adiyaman University
Turkey

Pedro Orihuela
Universidad de Santiago de Chile
Chile

Correspondence:
Ridhwan Abdul **WAHAB**:
ridhwan@iium.edu.my

Zainul Amiruddin **ZAKARIA**
zaz@ums.edu.my

Section Biological activity

Received: 7 September 2021
Accepted: 31 December 2021
Accepted corrected: 24 March 2023
Published: 30 January 2024

Citation:
Khan AYF, Ahmed QU, Khatib A, Ibrahim Z, Nipun TS, Natto HA, Saiman MZ, Zakaria ZA, Wahab RA Identification of cancer inhibitors from Hystrix brachyura bezoar extracts using LC-MS multivariate data analysis and in silico evaluation on Bcl-2, cyclin B/CDK1, VEGF and NM23-H1 **Bol Latinoam Caribe Plant Med Aromat** 23 (1): 41 - 60 (2024).
https://doi.org/10.37360/blacpma.24.23.1.4

Abstract: *Hystrix brachyura* bezoar is calcified undigested material found in the gastrointestinal tract known for various medicinal benefits including as an anticancer agent. However, the *H. brachyura* population has been declining due to its demand and is under Malaysian law protection. Therefore, present study aimed to identify bezoar anticancer active compounds through metabolomics and in-silico approaches. Five replicates of bezoar powder were subjected to extraction using different solvent ratios of methanol-water (100, 75, 50, 25, 0% v/v). Cytotoxicity and metabolite profiling using liquid chromatography-mass spectrometry were conducted. Putative compounds identified were subjected to in-silico analysis with targeted anticancer proteins namely, Bcl-2, Cyclin B/CDK1 complex, VEGF and NM23-H1. The correlation of LC-MS and cytotoxicity profile pinpointed two compounds, mangiferin and propafenone. *In-silico* study showed both compounds exerted good binding scores to all proteins with hydrophobic interaction dominating the ligand-protein complex binding, suggesting the ligands act as hydrophobes in the interactions.

Keywords: *Hystrix brachyura*; Anticancer; LCMS; Metabolomics; Molecular docking

Resumen: El bezpar de *Hystrix branchyura* es material calcificado sin digerir encontrados en el tracto gastrointestinal, conocido por sus variados beneficios médicos, incluyendo propiedades anticancerosas. De todas formas, la población de *H. Branchyura* ha ido declinando debido a su demanda y está bajo la protección de la ley de Malasia. Por esto, este estudio busca identificar los componentes activos anticancerosos del bezoar mediante abordajes metabolómico e in silico. Cinco réplicas de polvo de bezoar fueron sometidos a extracción usando solventes con diferentes proporciones metanol-agua (100, 75, 50, 25,0% v/v). Se hicieron perfiles de citotoxicidad y de metabolitos usando cromatografía líquida-espectrometría de masa (LC-MS). Se identificaron compuestos putativos yse sometieron a análisis in silico, buscando las proteínas anticancerosas Bcl-2, complejo Cyclin B/CDK1, VEGF, y NM23-H1. La correlación LC-MS y el perfil de citotoxicidad identificaron dos compuestos: mangiferina y propafenona. El estudio in silico mostró que ambos compuestos tenían buenos índices de enlace con todas las proteínas con interacción hidrofóbica dominando el enlace complejo proteína-ligando, sugeriendo que los ligandos actúan como hidrófobos en las interacciones.

Palabras clave: *Hystrix brachyura*; Anticancer; LC-MS; Metabolomica; Encaje molecular

INTRODUCTION

Hystrix brachyura (H. bracyura) is one of the common porcupine species that reside in South East Asia and it belongs to the Hystricidae family (Shan *et al*., 2019). Presently, according to the International Union for Conservation of Nature (IUCN) red list, the *H. brachyura* population has been in decline due to illegal hunting (Lunde *et al*., 2008). The main reason for the population declining is due to the medicinal properties of the porcupine meat and bezoars (Ahmad *et al*., 2012; Shan *et al*., 2019). The porcupine bezoar is a rare phytobezoar formed when undigested plant materials consumed by porcupine accumulates and calcifies inside its gastrointestinal tract (Chung *et al*., 2016). In recent years, studies have reported for *H. brachyura* bezoar to have antioxidant, antiviral and anticancer activities (Peng *et al*., 2018; Firus Khan *et al*., 2019a; Firus Khan *et al*., 2019b). Our previous study reported *H. brachyura* bezoar's effect on melanoma cancer cells (A375) in which it was found to exhibit anticancer activities by inducing apoptosis and cell arrest in G2/M phase (Firus Khan *et al*., 2019b). In another study, *H. brachyura* bezoar had been shown to inhibit angiogenesis and metastasis as well in A375 cells (Firus Khan *et al*., 2019a). Studies reported in the 21st century, every country has cancer as the leading cause of death and responsible for being the barrier to increasing life expectancy (Bray *et al*., 2018). Currently, the researchers aim to treat cancer and prolong patients' survival with advanced stage while preserving their quality of life (Bray *et al*., 2018; Prager *et al*., 2018) Therefore, research development has been guided by cancer hallmarks which have been suggested to target to induce cell death, disrupt proliferative signals, induce growth suppressors, inhibit invasion and metastasis, disable immortality replicative and inhibit angiogenesis cancer (Hanahan & Weinberg, 2000; Hanahan & Weinberg, 2011).

Following the cancer hallmarks, the present study focused on four proteins which are involved in anticancer activity, namely Bcl-2, cyclin B/CDK1 complex, VEGF and NM23-H1. The first protein, namely Bcl-2 protein, is a part of the Bcl-2 family which regulates cell death. Although Bcl-2 protein function is to inhibit apoptosis cascade by maintaining the mitochondrial membrane integrity, downregulation of Bcl-2 level in cancer cells has suggested that the cell's signalling has progressed into apoptosis (Hata *et al*., 2015). Therefore, by inducing apoptosis, it tackles one of the hallmarks of cancer by inducing cell death. The second protein, cyclin B/CDK1 complex is the key signalling when the cells are allowed to proceed into the mitosis phase from G2 phase in the cell cycle (Ha *et al*., 2017; Liu *et al*., 2019). Inhibition of the complex formation causes the cancer cells to get arrested in G2 phase which results in cells to stop proliferating (Coxon *et al*., 2017). Inhibition of the cyclin B/CDK 1 complex, targets another two hallmarks of cancer by disrupting cells proliferative signals and inducing growth suppressors.

The third protein involved directly with the angiogenesis process is vascular endothelial growth factor (VEGF) protein. VEGF promotes formation of new blood vessels to supply oxygenated blood in compromised blood circulation parts in the body (Lutfiya *et al*., 2019). However, in the case of cancer, VEGF aids in supplying oxygenated blood to local tumours, initiating angiogenesis cascade and cancer cells migrate to other parts of the body (Loizzi *et al*., 2017; Pandey *et al*., 2018). Therefore, inhibiting VEGF protein results in inhibiting angiogenesis and metastasis of cancer which is one of the cancer hallmarks. Furthermore, the fourth target protein, NM-23H1 also known as nucleoside diphosphate kinase is one of the metastasis suppressors in MAPK pathway signalling (Khan & Steeg, 2018). NM-23H1 had been reported have nucleoside diphosphate kinase (NDPK) activity, histidine protein kinase activity (HPK) and a 5′–3′exonuclease activity which resulted in metastasis inhibition (Prabhu *et al*., 2012; Yokdang *et al*., 2015). Hence, activating NM-23H1 target has been considered one of the cancer hallmarks by inhibiting cancer invasion and metastasis.

Our previous study had shown *H. brachyura* extracts exhibited anticancer effects on melanoma cells, A375 by inducing apoptosis, arrest cells in G2 phase, inhibit angiogenesis and metastasis (Firus Khan *et al*., 2019a). However, in our toxicity study, *H. brachyura* extracts exerted significant toxicity effects towards *Danio rerio* embryo (Firus Khan *et al*., 2020). Furthermore, *H. brachyura* bezoar is rarely found and poaching the *H. brachyura* in Malaysia is considered illegal as the porcupine comes under the protection of Malaysian law (Shan *et al*., 2019). Therefore, the aim of the present study was to characterize *H. brachyura* bezoar through LC-MS based metabolomics correlated with IC_{50} from

anticancer assay and evaluate identified active compounds with four target cancer proteins, namely Bcl-2, cyclin B/CDK1 complex, NM-23H1 and VEGF interaction using molecular docking approach. In this study, liquid chromatography (LC) coupled with quadrupole time-of-flight (Q-TOF) mass spectrometry (MS) based metabolomics was used to identify possible active compounds that correlate to anticancer activity of the *H. brachyura* extracts. The LC-MS is a highly sensitive analytical technique to detect with a wide range of polar and non-polar molecules that can be analysed without an involvement of the derivatization step and a small amount of sample is needed for the analysis (Nalbantoglu, 2016). Using the molecular docking approach, putative ligand-protein interaction can be predicted and further analysed with 2D and 3D diagrams to elucidate the interaction at the binding site.

MATERIALS AND METHOD

Chemicals and Materials

Hystrix brachyura bezoar (*H. brachyura)* is one of the protected materials according to Malaysian law. Permission from the Malaysian government authority, Department of Wildlife and National Parks, Malaysia was obtained (JPHL & TN (IP): 100-34/1.24 Jld 8) before conducting the study. The human melanoma cell (A375) line was acquired from the American Type Culture Collection (ATCC), USA. The A375 cells were grown in a complete growth medium (CGM) complemented with Dulbecco's modified Eagle medium, fetal bovine serum, and penicillin-streptomycin from Nacalai Tesque, Japan. Standard anticancer drug, fluorouracil (5-FU) was purchased from Sigma, the USA and used as the positive control. CellTiter 96® AQueous One Solution Cell Proliferation Assay kit was purchased from Promega, the USA and used for cytotoxicity assay. Analytical grade methanol used for the extraction process was procured from Merck, Germany.

Porcupine bezoar extract preparation for metabolomics

The *H. brachyura* bezoars were crushed into a fine powder using a mortar pestle. Subsequently, powder (300 mg) was extracted with ultrasonication method with different solvents, namely 100% water (A), 75% water: methanol (B), 50% water: methanol (C), 25% water: methanol (D) and 100% methanol (E). Five replicates of *H. brachyura* for each solvent were sonicated for 30 minutes, filtrates were filtered and oven-dried (40℃) and kept at -80 ℃ before further investigation.

Cytotoxicity of porcupine bezoar extracts on A375 cells

The cytotoxicity of *H. brachyura* extracts was performed on A375 cells by determining the 50% inhibitory concentration (IC_{50}) using MTS kit following the manufacturer's instruction. A375 cells were exposed to *H. brachyura* extracts for 72 h before being measured by MTS kit for the analysis of IC_{50} using GraphPad Prism software version 7.

Metabolites profiling using Q-TOF Liquid Chromatography-Mass Spectrometry (Q-TOF LC-MS)

The Q-TOF LC-MS analysis was performed to detect metabolites which were soluble in liquid, non-volatile and thermally fragile molecules present in *H. brachyura* extracts as described previously (Nipun *et al*., 2020). A Q-TOF LC-MS system of Agilent 1290 Infinity and 6550 iFunnel Q-TOF LC-MS equipped with an electrospray interface (ESI) with both positive and negative ions mode was used to analyse samples. Two mg of each sample was vortexed with 200 µL of 1:1, methanol: water to ensure full dissolution before being filtered and transferred into the glass vials. The samples were then injected to a Phenomenex Kinetex C_{18} core-shell technology 100 Å (250 x 4.6 mm, 5µ) column, equilibrated with methanol. Samples were eluted with a gradient system from 5% methanol in water with 0.1% formic acid to absolute methanol in 20 min, then with absolute methanol for 10 min and then decrease to 5% methanol for another 15 min at a flow rate of 0.7 mL/min with a total acquisition time of 45 min. All metabolites detected by Q-TOF MS operated in electrospray ionization (ESI) at positive mode. The MS/MS data were collected in the range of m/z 100 to 1700 with the scan rate of a spectrum/ scan. The MS/MS spectra were obtained by a collision energy ramp of 30 to 35 eV. The Q-TOF LC-MS data acquired were subjected to analysis with ACD/Spec Manager v.12 by converting the raw files into netCDF (*.cdf) formats. The Q-TOF LC-MS data was then pre-processed using XCMS software packaged with R version 2.15.1 language for

filtering, identifying, matching, filling the peaks, retention time correction and saving in csv format. The results were analysed with the SIMCA-P$^+$ 14.0 program for multivariate data analysis.

Molecular docking analysis

The molecular docking analysis was performed to predict the interaction between active compounds detected from Q-TOF LC-MS metabolomics multivariate analysis with proteins responsible for anticancer activity. The 3D structure of ligands was obtained from PubChem (National Centre for Biotechnology Information (NCBI), USA in SDF format and converted into PDB format using Avogadro software. The ligands were prepared into PDBQT format after Gasteiger charges were added, the rotatable bonds in the ligand were assigned with AutoDock Vina 1.1.2 software and all torsions were allowed to rotate. Our previous study reported *H. bracyura* extracts exert anticancer effects by inducing apoptosis, arresting cells in G2 phase, inhibiting angiogenesis and metastasis. Therefore, crystallographic structure of proteins related to anticancer activity viz. anti-apoptosis Bcl-2 (PDB ID: 2W3L), G2 phase arrest cyclin B/CDK1 complex (PDB ID: 6GU2), vascular endothelial growth factor responsible for angiogenesis (PDB ID: 1FLT) and metastasis suppressor protein, NM-23 (PDB ID: 1NUE) were obtained from Protein Data Bank (PDB) of *Homo sapiens* species as receptors. The receptors were prepared into PDBQT using AutoDock Vina 1.1.2 by removing water, molecules, added hydrogen to the polar end, merged with non-polar and conditioned with a pH of 7.4 using PDB2PQR Server, version 2.0.0 to mimic the actual condition of the assay media. The docking grid box was set to center the receptor and covered the whole receptor. The docking analysis was conducted using AutoDock Vina 1.1.2 software. The best conformations with the highest binding affinity (the more negative value) were selected as the best-docked model. The 3D superimposed diagram of the complex was developed using PyMOL ™ 1.7.4 and 2D interaction was analysed using Ligplot$^+$ software produced.

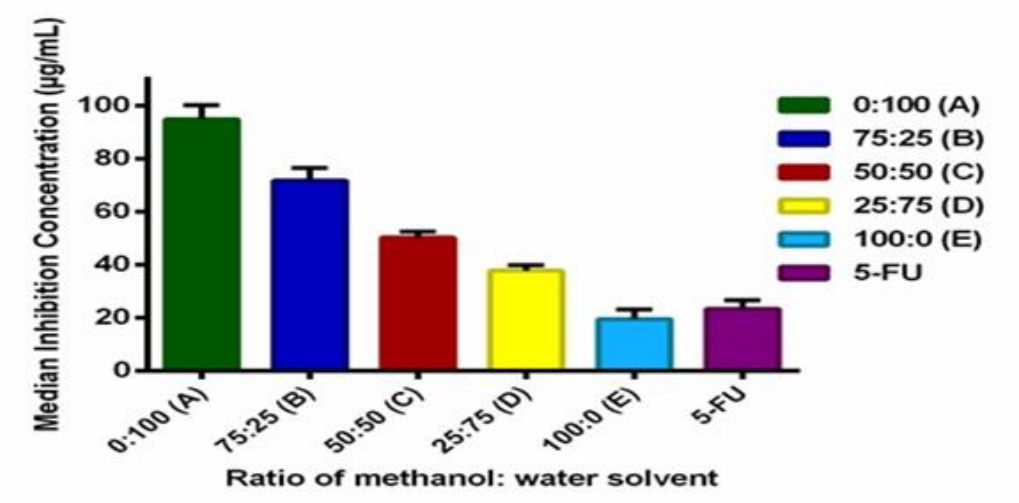

Figure No. 1

Effect of median solvent concentration of cytotoxic assay on A375 cells of *H. brachyura* extracts. Data expressed as mean ± SD (n=5). Note: 100% water (A) extract, 75% water: methanol (B) extract, 50% water: methanol (C) extract, 25% water: methanol (D) extract, 100% methanol (E) extract and fluorouracil (5-FU)

RESULTS

H. brachyura cytotoxicity analysis

Figure No. 1 presents the IC_{50} of A375 cells treated with various concentrations of methanol: water *H. brachyura* extracts. The finding demonstrated that the polarity of the solvents played a role in exerting cytotoxicity activity with non-polar solvents, E (19.5 µg/mL) had the highest cytotoxicity activity, followed by D (37.7 µg/mL), C (50.2 µg/mL), B (71.7 µg/mL) and A (94.8 µg/mL). Two extracts,

namely D and E had higher cytotoxicity activity compared to other extracts as their IC_{50} value < 50 µg/mL.

Multivariate Data Analysis

The multivariate data analysis was used to correlate cytotoxic activity (IC_{50}) with Q-TOF LC-MS data to evaluate the potential active compounds of *H. brachyura* extracts (A, B, C, D and E) on A375 cells. The OPLS model was used to discriminate the *H. brachyura* extracts metabolites. Mass to charge ratio (m/z) and IC_{50} of the cytotoxic assay was used as OPLS component 1 and OPLS component 2 and as x and y variables respectively.

Figure No. 2 presents the score scatter plot and summary of the fit of the extracts generated from the Q-TOF LC-MS positive ionization data. Figure No. 2A displays the distribution of the metabolites based on the OPLS components 1 and 2 in which the active and less active extracts can be seen as separated. The score scatter plot demonstrated the active extract, E and D distributed on the positive quadrant, whereas C, B and A on the negative quadrant. Figure No. 2B shows a summary of the fit for Q-TOF LC-MS metabolites OPLS model. The OPLS component 1 explained 78.3% of variation while OPLS component 2 explained 7.4% variation. The OPLS model was verified for its goodness of fit and predictive ability using the permutation test. The intercept of R^2Y and Q^2Y for the Q-TOF LC-MS with positive ionization in this study was found to be acceptable when the cumulative values of both R_2Y and Q_2Y were greater than 0.5 as R^2 was around 0.4 while Q2 was -0.289 (Eriksson *et al.*, 2013). The finding suggested the OPLS model for Q-TOF LC-MS metabolites was valid.

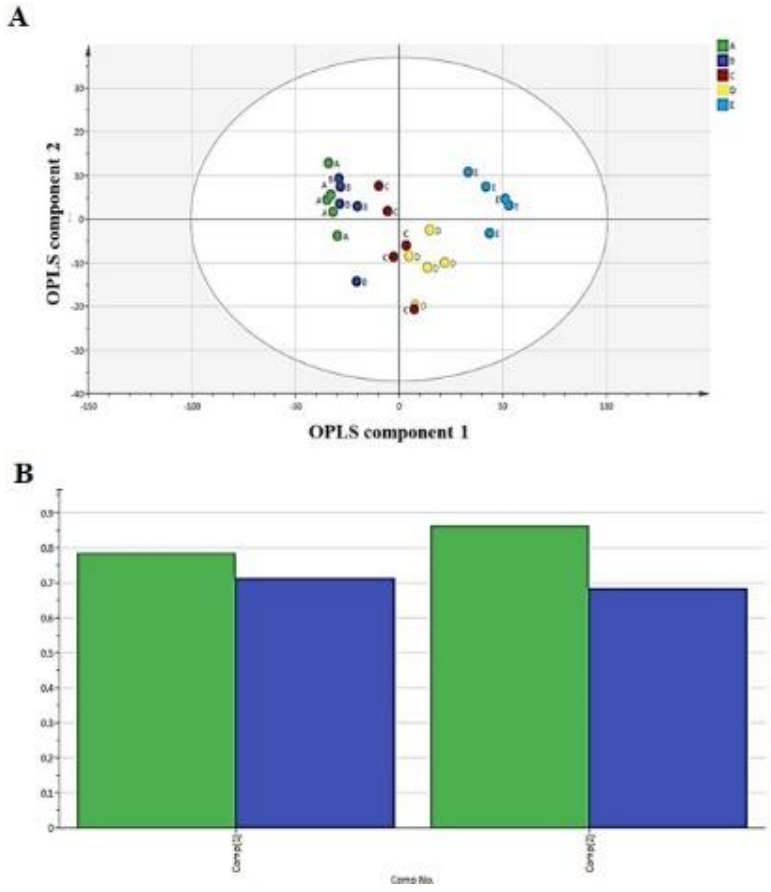

Figure No. 2
(A) The score plot of different extracts of *H. brachyura* extracts (A, B, C, D and E) based on the OPLS model. (B) The summary of fit of the OPLS model of the *H. brachyura* extracts

Figure No. 3 demonstrates the loading scatter plot of the *H. brachyura* methanol extract and metabolites identified as potential active compounds for *H. brachyura* anticancer activity. Figure No. 3A displays the correlation of m/z, the x variable to IC_{50}, the y variable where the *m/z* values closer to IC_{50} designates positive correlation to cytotoxicity on A375 cells. The present study was able to identify two metabolites, namely propafenone and mangiferin by comparing the metabolites fragments ions with available databases. Figure No. 3B shows the chemical structure of propafenone and mangiferin.

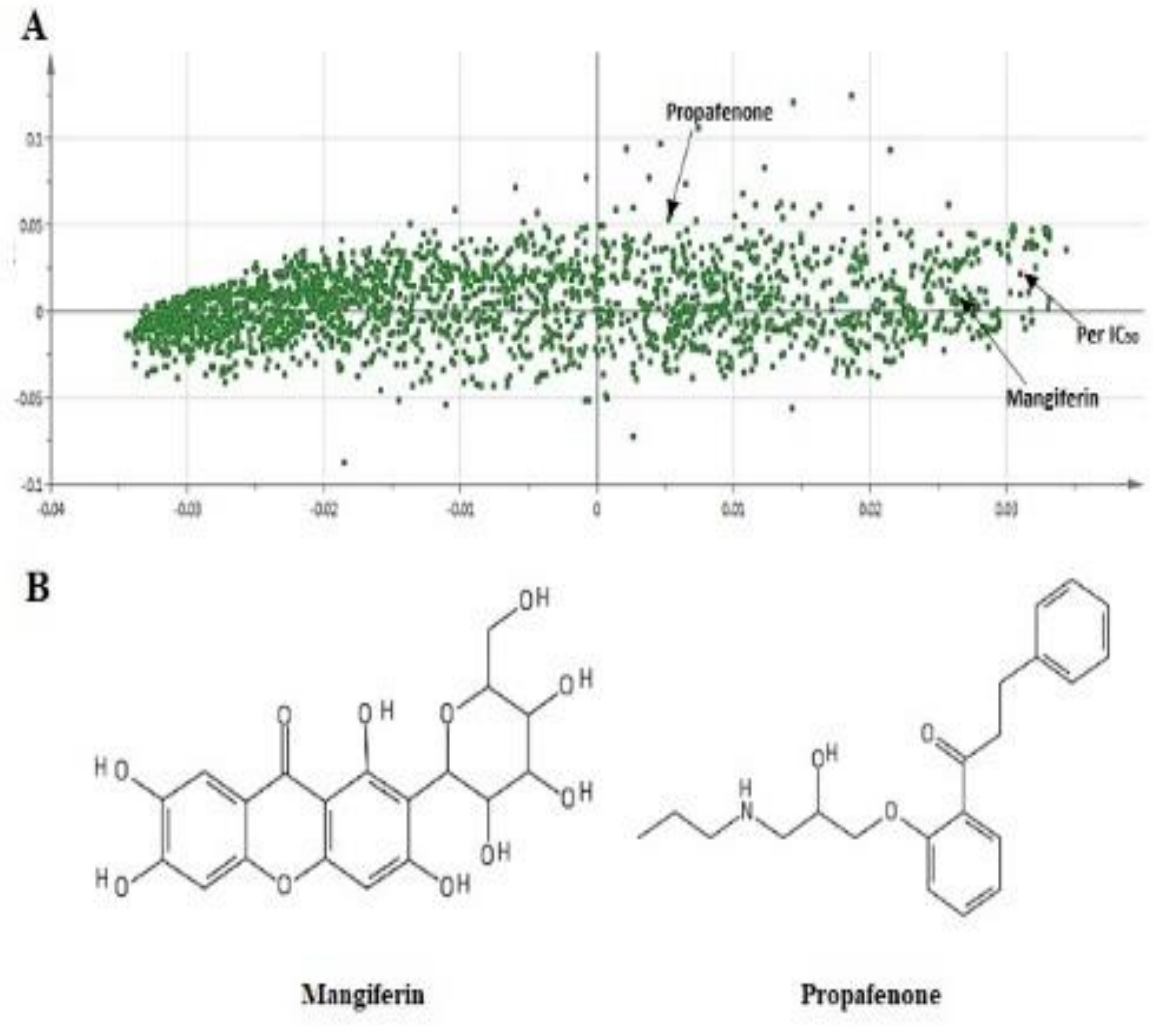

Figure No. 3
(A) The loading scatter plot of OPLS model of the *H. brachyura* methanol extract analysed using Q-TOF LC-MS with positive ionization. (B) Metabolites identified as potential active anticancer agents from *H. brachyura* methanol extract

Structure elucidation of identified metabolites

Elucidating the chemical structure of parent ions was performed using MSMS fragmentations technique. The MSMS fragmentations for both metabolites are reported in Table No. 1. The metabolites were confirmed by comparing with the reported literature, databases and analysis of the ion fragmentation.

Table No. 1
Tentative anticancer metabolites identified in the *H. brachyura* methanol extract through Q-TOF LC-MS/MS fragmentation using positive ionisation mode

No	M+H	MS^2 fragments ions	Tentative metabolites	Reference
1	423.1	[M- H O]$^+$ at m/z 405, [M- $C_4H_9O_3$]$^+$ at m/z 317, [M- $C_3H_9O_5$]$^+$ at m/z 297, [M- $C_5H_{11}O_5$]$^+$ at m/z 271, [M- $C_5H_{13}O_5$]$^+$ at m/z 269, [M- $C_6H_{13}O_6$]$^+$ at m/z 241 and [M- $C_{12}H_{13}O_7$]$^+$ at m/z 153	Mangiferin	Gold-Smith *et al*., 2016 Khurana *et al*., 2016
2	342.2	[M- H_6O]$^+$ at m/z 319, [M- C_3H_5]$^+$ at m/z 300, [M- C_3H_7]$^+$ at m/z 298, [M- C_3H_8]$^+$ at m/z 297, [M- C_3H_9N]$^+$ at m/z 282, [M- $C_3H_6O_2$]$^+$ at m/z 267, [M- $C_4H_{12}O$]$^+$ at m/z 265, [M- $C_5H_{12}NO$]$^+$ at m/z 239, [M- $C_5H_{13}NO_2$]$^+$ at m/z 222, [M- $C_6H_{16}NO_2$]$^+$ at m/z 207 and [M- $C_{10}H_{14}O$]$^+$ at m/z 191	Propafenone	Schwarz *et al*., 2016 Balik *et al*., 2017

Mangiferin consists of a pyran, two benzene rings attached to a glucosyl unit with eight hydroxyl (OH) and a ketone (C=O) functional groups which indicate the xanthone is the parent chain. In the positive ionisation mode (ESI), mangiferin was protonated at the hydroxyl functional group to form the parent ion $(M+H)^+$ of m/z: 423. The compound underwent rearrangement and subsequently eliminated OH, $C_4H_9O_3$, $C_3H_9O_5$, $C_5H_{13}O_5$, $C_6H_{13}O_6$, $C_5H_{11}O_5$ and $C_{12}H_{13}O_7$ respective fragments from the parent ion and consequently produced ions of m/z 405, 317, 297, 271, 269, 241, and 153, respectively. The pyran rearrangement and loss of water from the ion of m/z 423 led to the formation of the ion of m/z 405 followed by loss of $C_4H_8O_2$ from the parent ion produced m/z 317. Protonated parent ion underwent a loss of water producing m/z 405 ions. The parent ion of m/z 405 then fragmented to produce an ion of m/z 387 by removing another water molecule before undergoing another rearrangement to further fragmentation to produce an ion of m/z 357 which was produced from the loss of CH_2O from the parent ion. The ion m/z 357 subsequently fragmented to an ion of m/z 297 due to the loss of $C_2H_4O_2$. Protonated parent ion m/z 423 underwent pyran rearrangement into a chain of carbon with 5 hydroxyl groups before undergoing fragmentation into an ion of m/z 271 due to the loss of $C_{14}H_7O_6$. The parent ion m/z 423 produced another ion m/z 405 due to the loss of water at C6 and C7. The ion is further fragmented into m/z 241 by removing $C_6H_{12}O_5$ from the parent ion. Protonated ion fragmented producing m/z 153 due to the loss of $C_{19}H_{19}O_{11}$ from the parent ion.

Propafenone is an aromatic ketone that consists of 3-(propylamino) propane-1,2-diol and 2-(3-phenylpropanoyl) phenyl as a substituent. In the positive ionisation mode (ESI), propafenone was protonated at amine to form the parent ion $(M+H)^+$ of m/z 342. Propafenone underwent rearrangement and subsequently removed H_6O, C_3H_5, C_3H_7, C_3H_8, C_3H_6N, $C_3H_{12}O$, $C_5H_{12}N_O$, $C_5H_{13}NO_2$, $C_6H_{16}NO_2$, and $C_{10}H_{14}O$ from the parent ion that produced as a consequence the ions of m/z 319, 300, 298, 297, 282, 267, 265, 239, 222, 207 and 191, respectively. The protonation of propafenone at the N-H attached to its amine group formed the parent ion $(M+H)^+$ of m/z 342. The loss of water from the parent ion formed an ion of m/z 324 which was further deprotonated thrice to produce an ion of m/z 321 and deprotonated twice further forming an ion of m/z 319. From the protonated parent ion of m/z 342, propene was fragmented at the 3-propylamino forming an m/z 300

parent ion. The ion of m/z 297 was formed as the parent ion of m/z 300 fragmented to an ion of m/z 297 by undergoing deprotonation thrice at the amine group. While ion m/z 282 was resulted from the parent ion of m/z 342 due to the loss of propylamino before undergoing rearrangement and deprotonation to form an ion of m/z 282. Additionally, ion of m/z 267 was fragmented from the parent ion of m/z 342 as the parent ion underwent a series of McLafferty rearrangement before being fragmented to $C_3H_7O_2$ to produce an ion of m/z 267. Protonated parent ion underwent rearrangement to its 3-propylamino before being fragmented into an ion of m/z 326 due to the loss of CH_4, into an ion of m/z 308 due to the loss of water and into an ion of m/z 265 due to the loss of C_3H_7. The loss of $C_5H_{15}NO$ from the parent ion produced an ion of m/z 239 before being further fragmented due to the loss of hydroxyl group producing an ion of m/z 222. Protonated parent ion is further fragmented into an ion of m/z 225 due to the loss of $C_6H_{15}NO$ and subsequently into an ion of m/z 207 from the loss of water. The protonated parent ion further underwent fragmentation due to the loss of water, loss of C_3H_6 from propylamino and C_7H_7 from benzene ring to produce ions of m/z 324, 282 and 191, respectively.

Molecular docking

Molecular docking analysis was performed to elucidate the interaction between identified metabolites with the targeted anticancer proteins. Ligand binding to the receptor induces a change in the intracellular region that promotes adapter proteins activation and death-inducing signalling complex formation. Table No. 2 presents binding affinity of ligand-receptor interaction between control ligand, mangiferin and propafenone with Bcl-2, cyclin B/CDK1 complex, VEGF and NM-23H1 proteins. Lower binding affinity indicates a higher docking score, has the highest activity and favourable binding interaction. Bcl-2 is one of the anti-apoptosis proteins, ligands binding with Bcl-2 promotes inhibition of Bcl-2 to function which results in apoptosis to progress. The results in Table No. 2 show navitoclax, Bcl-2 inhibitor drug, exhibited the lowest binding affinity of -11.5 kcal/mol compared to the remaining ligands. Mangiferin showed lower binding affinity (-8.2 kcal/mol) compared to propafenone (-7.2 kcal/mol) indicating that both ligands had a good binding score in inhibiting Bcl-2. The cyclin B/CDK1 complex (also known as maturation promoting factor or MPF) is one of the main protein kinases that gets stimulated and aids as master regulator for the mitosis-phase transition, phosphorylating and activating other downstream protein kinases, and directly posphorylating several structural proteins involved in cellular reorganization. The ligand binds to the cyclin B/CDK1 complex and acts as an inhibitor. Alvocidib, the cyclin B/CDK1 inhibitor and control ligand in this study showed a promising binding score with a binding affinity of -9.6 kcal/mol. Both ligands displayed a good binding score with low binding affinity energy of -8.2 and -8.0 kcal/mol for propafenone and mangiferin, respectively.

Table No. 2

Molecular interaction results of targeted protein with control and the active ligands. The control ligand used for Bcl-2 is navitoclax, alvocidib for cyclin B/CDLK 1 complex, squalene for VEGF and isolinderalactone for NM-23 protein

Ligands	Binding affinity (kcal/mol)			
	Bcl-2	Cyclin B/CDK1 complex	VEGF	NM-23
Navitoclax	-11.5	-	-	-
Alvocidib	-	-9.6	-	-
Squalene	-	-	-7.5	-
Isolinderalactone	-	-	-	-6.7
Mangiferin	-8.2	-8.0	-7.5	-7.8
Propafenone	-7.2	-8.2	-7.4	-6.7

Vascular endothelial growth factor (VEGF) is a signal protein produced which stimulates the formation of blood vessels. Hence, ligands binding to the protein considered as VEGF inhibitor which promotes angiogenesis inhibition. Squalene, the control docking used for VEGF protein docking displayed -7.5 kcal/mol binding affinity. Mangiferin and propafenone showed a good binding score as well as both ligands exerted low binding affinity with nearly the same binding score as squalene viz. -7.5 kcal/mol for mangiferin and -7.4 kcal/mol for propafenone. NM23-H1 is one of the proteins which signals metastasis suppressor for cancer cells, hence, good binding with the protein promotes metastasis inhibition. The control docking ligand, isolinderalactone showed a moderate binding score of binding affinity of -6.7 kcal/mol. Mangiferin on the other hand displayed a lower binding affinity i.e., -7.8 kcal/mol compared to isolinderalactone suggesting better ligand to suppress cancer metastasis. However, propafenone showed a similar binding affinity with control docking for NM23-H1 protein -6.7 kcal/mol.

Figure No. 4 presents 2D ligand-receptor interaction and a superimposed 3D image of the interaction for Bcl-2 protein. Mangiferin in Figure No. 4A is demonstrated to have eight hydroxyl groups and a carbonyl group which tend to form hydrogen bonds with residues viz. ARG26, LYS22, SER64, SER75, TYR161 and ALA159. Moreover, the carbons from pyran and two benzene rings of mangiferin contribute in establishing 13 hydrophobic interactions with GLY104, VAL107, PHE71, VAL115, VAL118, ARG66, PHE63, ASP62, ARG26, SER64, SER75, TYR161 and ALA159 amino acid residues. On the other hand, propafenone in Figure No. 4B shows that ligand-receptor interaction consists of only one hydrogen bond viz. VAL92 interacts with hydroxyl groups. Propafenone dominantly exhibited hydrophobic interaction with residues instead of the hydrogen bond interaction. Moreover, the ligand structure combination of aromatic hydrocarbon chains contributed to hydrophobic interaction viz. GLU95, ALA108, LEU96, PHE112, PHE71, TYR67, ASP70, PHE63, MET74 and VAL92. These groups were largely responsible for forming stable receptor-ligand complexes, hence having a high binding affinity score. The superimposed diagram displayed mangiferin binds inside the active site together with navitoclax suggesting it behaved as a competitive inhibitor. On the other side, propafenone binds in the allosteric site, indicating it as a non-competitive inhibitor.

Figure No. 5 demonstrates the 2D ligand-receptor interaction and superimposed 3D image of the interaction for cyclin B/CDK1 complex protein. The 2D diagram in Figure No. 5 reveals that mangiferin and propafenone receptor-ligand interaction is predominantly by hydrophobic interaction. Mangiferin in Figure No. 5A shows six hydrogen bonds with four amino acid residues, namely ASP86, LYS89, LEU83, and LYS33 with its hydroxyl group. Furthermore, the hydrophobic structure which is the hydrophobes characteristic composed of 12 hydrophobic interactions with SER84, MET85, LEU135, VAL64, PHE80, VAL18, ILE10, GLY11, ASP86, LYS89, LEU83 and LYS33 amino acid residues to stabilize the binding. Propafenone (Figure No. 5B) had a lower binding affinity compared to mangiferin. Hence, it was considered to have a higher binding score in inhibiting cyclin B/CDK1 protein. The hydroxyl group formed two hydrogen bonds with VAL336 and PHE338 while the nitrogen contributed another hydrogen bond with HIS337 amino acid residue. In addition, propafenone carbon backbone structure played a major role in having low binding affinity and aided in forming the significant hydrophobic interactions with GLU181, PRO339, ALA185, GLU182, GLN184, PRO340, VAL186, SER227, PRO301, ASP230, VAL226, TYR223, THR329, ILE343, MET330, HIS337, VAL336 and PHE338 amino acid residues. From the superimposed diagram in Figure No. 5C, mangiferin interaction for cyclin B/CDK1 protein showed binding inside the active site to stabilize the complex. Hence, it is a competitive inhibitor as alvocidib is bound in the active site as well. While propafenone acted as a non-competitive inhibitor as it bound in the allosteric site.

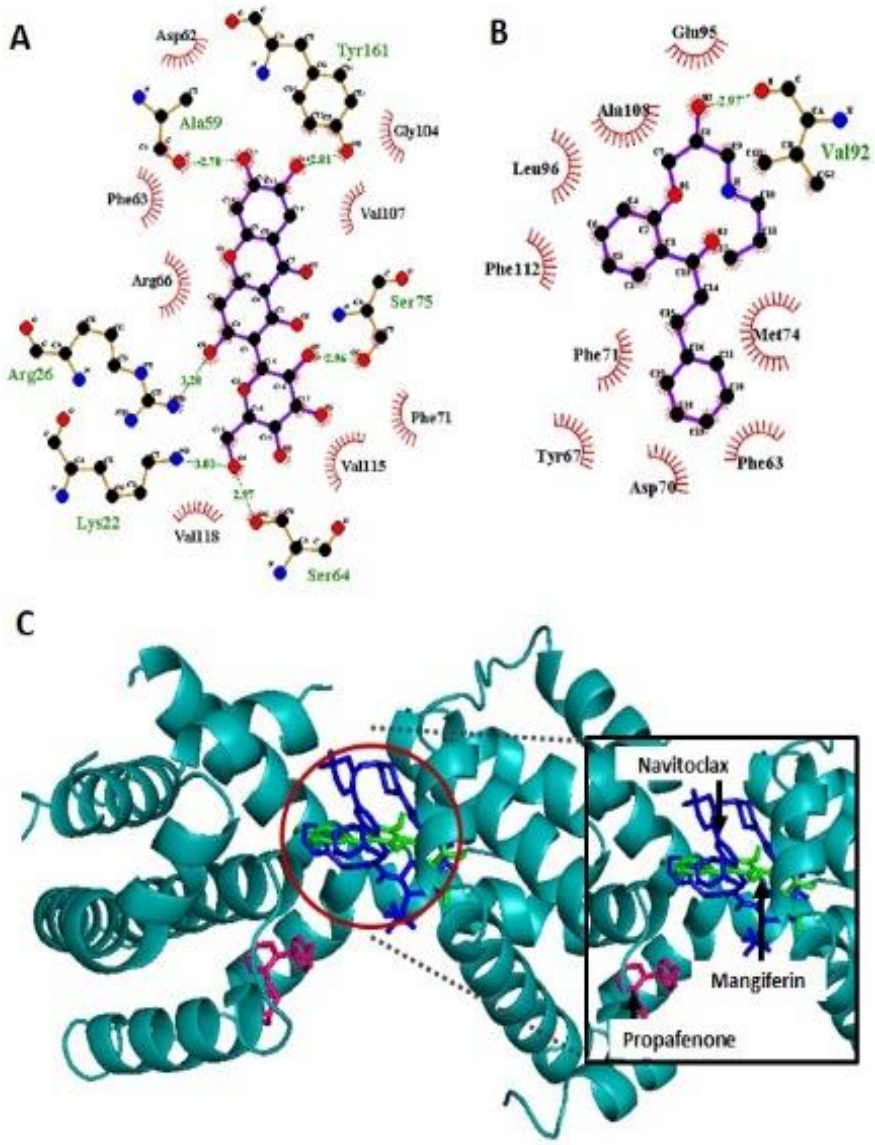

Figure No. 4

The 2D diagram of the protein-ligand interactions with the amino acid residues of Bcl-2 and identified ligands. A- Mangiferin, B- propafenone. The brown stick model indicates important amino acid residues near the binding site, purple stick model indicates the ligand, green dotted lines represent hydrogen bonds and the half-moon dashed indicates hydrophobic contact between amino acid residue and ligand. C- The superimposed 3D diagram showing the binding sites of ligands on Bcl-2 protein. The red circle indicates the location of the active site on the protein

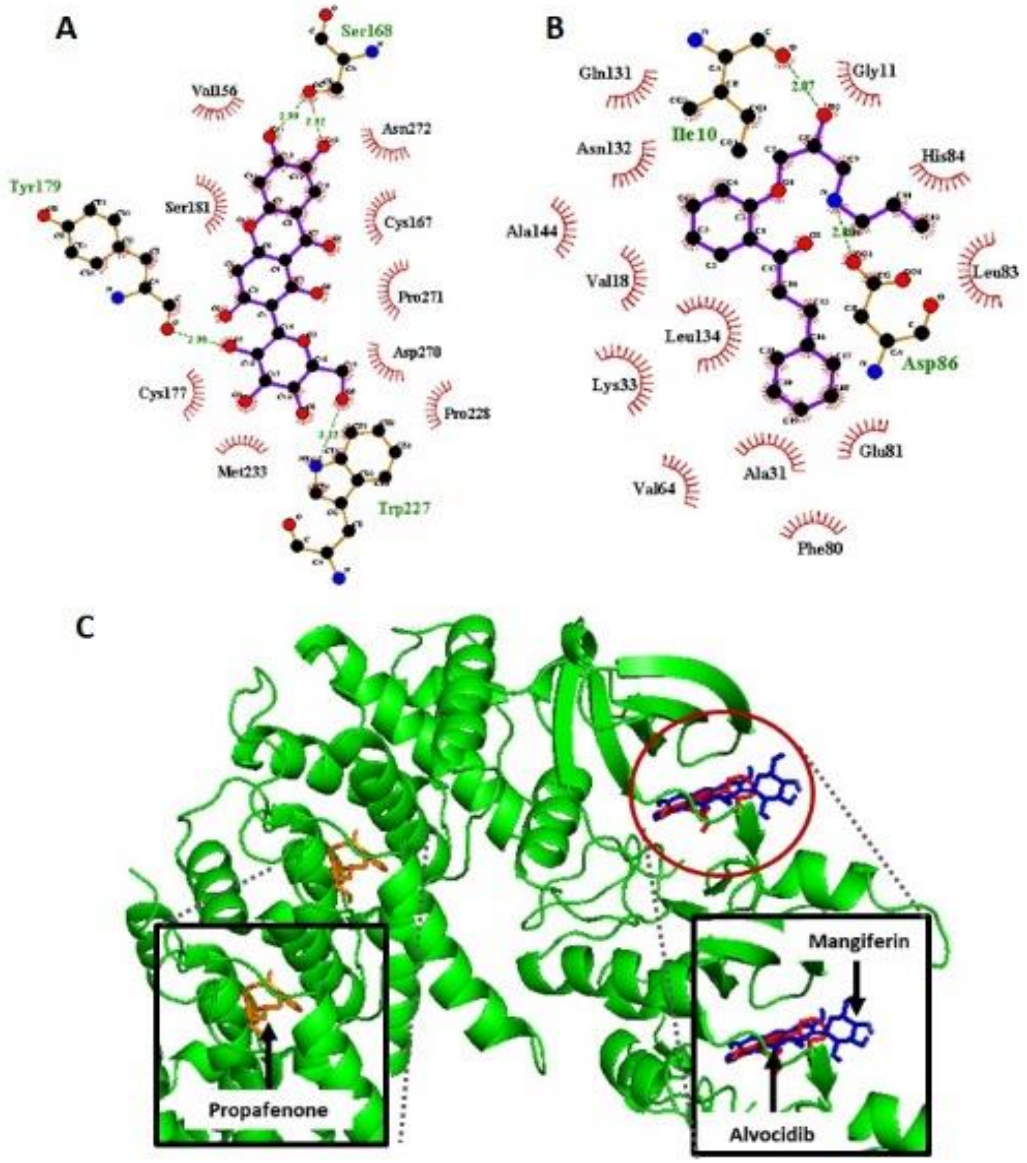

Figure No. 5

The 2D diagram of the protein-ligand interactions with the residues of cyclin B/CDK1 complex and identified ligands. A- Mangiferin, B- propafenone. The brown stick model indicates important residues near the binding site, the purple stick model indicates the ligand, green dotted lines represent hydrogen bonds and half-moon dashed indicate hydrophobic contact between residue and ligand. C- The superimposed 3D diagram showing the binding site of ligands on cyclin B/CDK1 complex protein. The red circle indicates the location of the active site on the protein

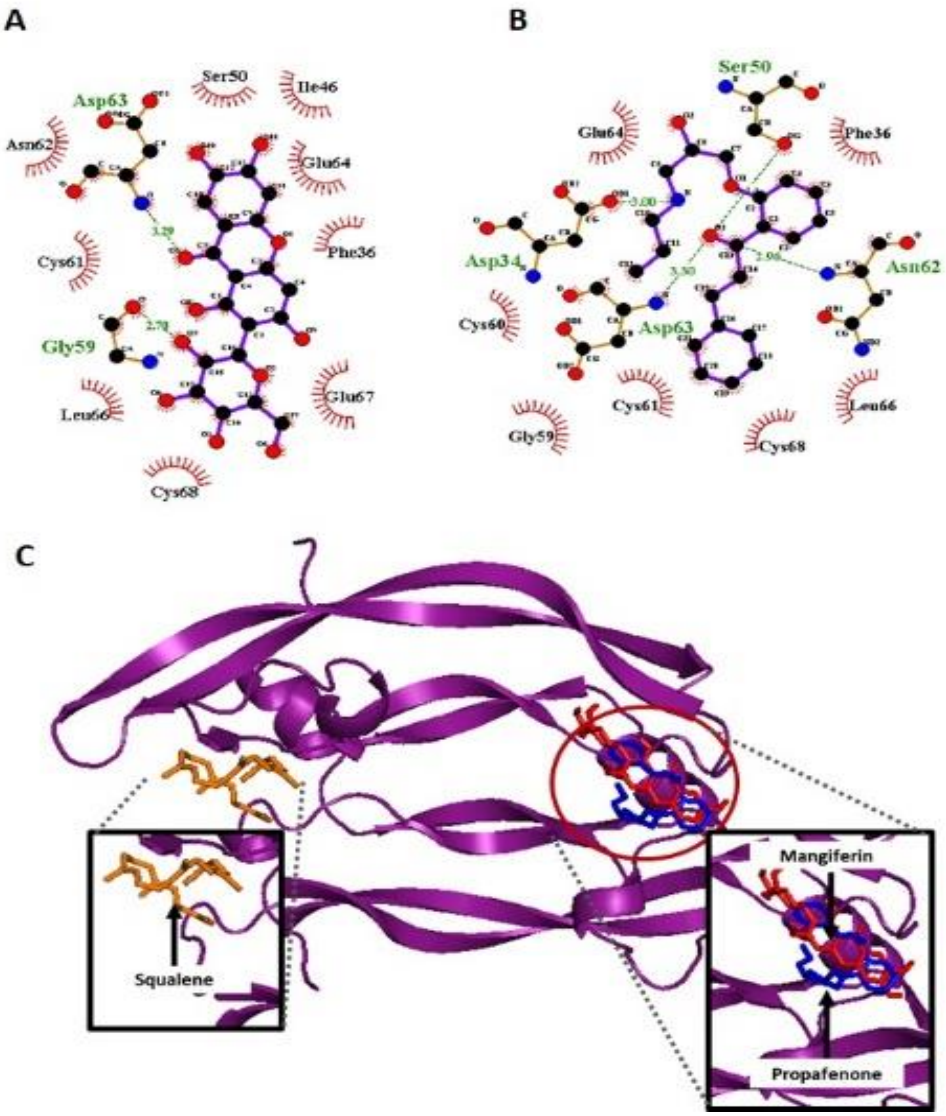

Figure No. 6

The 2D diagram of the protein-ligand interactions with the residues of VEGF and identified ligands. A- Mangiferin, B- propafenone. The brown stick model indicates important residues near the binding site, purple stick model indicates the ligand, green dotted lines represent hydrogen bonds and the half-moon dashed indicate hydrophobic contact between residue and ligand. C- The superimposed 3D diagram showing the binding site of ligands on VEGF protein. The red circle indicates the location of the active site on the protein

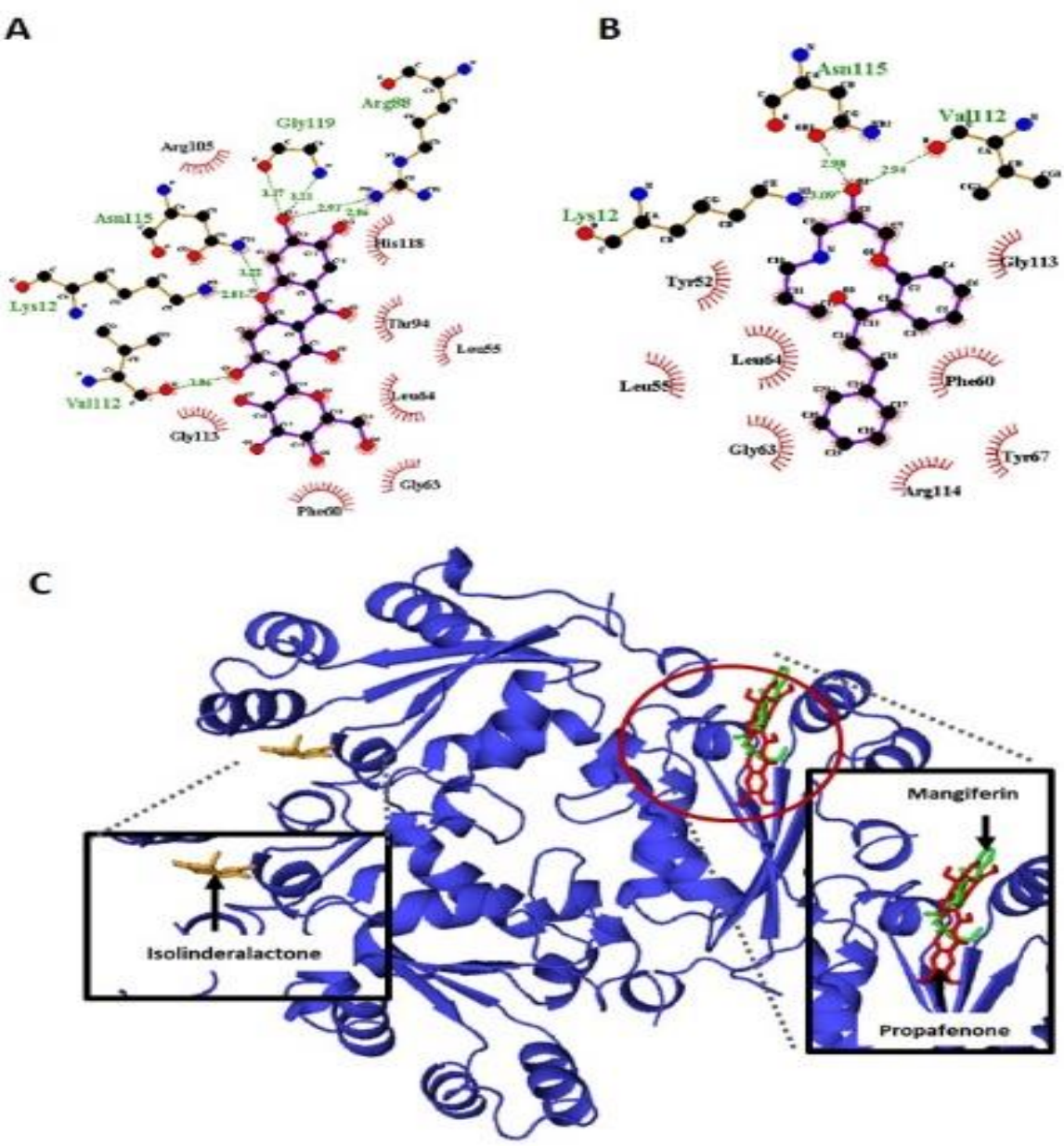

Figure No. 7

The 2D diagram of the protein-ligand interactions with the residues of NM23-H1 and identified ligands. A- Mangiferin, B- propafenone. The brown stick model indicates important residues near the binding site, purple stick model indicates the ligand, green dotted lines represent hydrogen bonds and the half-moon dashed indicate hydrophobic contact between residue and ligand. C- The superimposed 3D diagram showing the binding site of ligands on NM-23H1 protein. The red circle indicates the location of the active site on the protein

Figure No. 6 demonstrates a 2D diagram of molecular interaction involved in ligand-receptor binding of mangiferin (A) and propafenone (B) for VEGF protein. In the structure of mangiferin, hydrophobic interactions were seen with 11 amino acid residues viz. LEU66, CYS68, GLU67, PHE36, GLU64, ILE46, SER50, ASN62, CYS61, ASP63 and GLY59. Surprisingly, though mangiferin contains eight hydroxyl groups, it only formed two hydrogen bonds with ASP63 and GLY59 amino acid residues. Furthermore, propafenone formed 11 hydrophobic interactions with GLU64, PHE36, LEU66, CYS68, CYS61, GLY59, CYS60, ASP34, ASP63, ASN62 and SER50 amino acid residues while the nitrogen formed a hydrogen bond with ASP34 amino acid residue. The carbonyl functional group at C1′ formed three hydrogen bonds with SER50, ASP63, ASN62 amino residues. Figure No. 6C displays the superimposed ligands receptor diagram of VEGF. The diagram shows mangiferin and propafenone bind inside the active site while squalene binds in the allosteric site. The finding suggested that both the ligands were non-competitive inhibitors in stabilizing the binding for VEGF protein.

Interaction between NM-23H1 protein and mangiferin stabilized its molecular interaction at catalytic sites by forming seven hydrogen bonds and 12 hydrophobic interactions as shown in Figure No. 7A. A hydrogen bond formed between the hydroxyl group and VAL112 amino acid residue, two hydrogen bonds with ASN115 and LYS 12 amino acid residues with hydroxyl group. Additionally, GLY119 amino acid residue formed two hydrogen bonds with hydroxyl and ARG88 amino acid residue formed another two hydrogen bonds with oxygen at two different carbon backbone. Moreover, the carbons and hydroxyl groups of mangiferin formed 11 hydrophobic interactions, namely ARG105, HIS118, THR94, LEU55, LEU64, GLY63, PHE60, GLY113, VAL112, LYS12, ASN115 and ARG88 amino acid residues. Residue LEU55 was shown to have interaction as well with the carbonyl group. As for the propafenone, the molecular interactions were seen as three hydrogen bonds (ASN115, VAL112, LYS12) formed with a hydroxyl group. The carbon of propafenone contributed in forming 11 hydrophobic interactions involving GLY113, PHE60, TYR67, ARG114, GLY63, LEU64, LEU55, TYR52, LYS12, ASN115 and VAL112 amino acid residues. Similarly to VEGF interaction, mangiferin and propafenone showed binding inside the catalytic site while control docking ligand showed binding in the allosteric site. The diagram in Figure No. 7C demonstrated mangiferin and propafenone were non-competitive inhibitors when bounded with NM-23H1.

DISCUSSION

The process of bezoar formation in *H. brachyura* stomach may take several years to undergo complete calcification (Shan *et al*., 2019). With the complexity of bezoar nature and method of accessing the bezoar, *H. brachyura* bezoar usage as a whole is neither considered sustainable for standardization process nor commercialization purpose, thereby identifying the bioactive compounds for anticancer effects is necessary. Hence, the present study was performed to evaluate the anticancer activity, LC-MS metabolomics profiling of *H. brachyura* bezoar extracts prepared using various solvents and *in silico* investigation of active compounds identified with selected cancer proteins involved in anticancer activity. The result demonstrated solvents polarity played an essential role in the cytotoxicity whereby methanol extract's (E) cytotoxicity activity was the highest and the water extract had the least cytotoxicity activity. The finding was found to be in line with a previous study that reported *L. indica* leaf methanol extract had the highest cytotoxicity activity on DU-145, PC-3, and MEF-L929 cells compared to *L. indica* leaf aqueous extract (Ghagane *et al*., 2017). This was suggested due to the fact that methanol consists of both polar and non-polar functional groups, hence it had a great ability to extract both polar and non-polar compounds to exert anticancer activity (López-Perea *et al*., 2019).

Multivariate data analysis of Q-TOF LCMS metabolomics helped in identification of the two bioactive compounds, namely mangiferin and propafenone which were found to correlate with the cytotoxicity activity on A375 cells. Mangiferin is a bioactive ingredient predominantly isolated from the mango tree. It has been reported to exert a wide range of promising pharmacological effects including antioxidant, hypolipidemic, anti-inflammatory, neuroprotective, immunomodulatory, antibacterial, anti-viral, hepatoprotective and anticancer effects (Li *et al*., 2013; Khurana *et al*., 2016; Du *et al*., 2018). Mangiferin was reported to induce apoptosis by down-regulating Bcl2, Bcl-XL and upregulating caspase 3, caspase 9 and caspase 7 suggesting to

exert its effect through mitochondria-mediated pathway (Gold-Smith *et al*., 2016). In addition, in another study, mangiferin had been reported to inhibit cancer metastasis and angiogenesis (Du *et al*., 2018). Another bioactive compound identified to correlate with the cytotoxicity on A375 cells was propafenone. Propafenone is a class 1C antiarrhythmic medication commonly used for the treatment of arrhythmias which treats rapid heartbeats such as atrial and ventricular arrhythmias (Stoschitzky *et al*., 2016). A study conducted in 2017 reported for propafenone to exhibit its anticancer activity by inducing apoptosis, inhibiting cells growth of esophageal squamous cell carcinoma without exerting toxicity on normal esophageal cells and reducing mitochondrial membrane potential by decreasing the expression of Bcl-xL and Bcl-2 (Zheng *et al*., 2017).

Molecular docking of both identified compounds was performed to elucidate the interaction of the compounds with the targeted proteins at molecular level. The *Homo sapiens* anti-apoptotic protein Bcl-2 composed of homology domains (BH1, BH2, BH3 and BH4) builds from 288 residues and the BH3 domain accommodates hydrophobic binding groove which is considered as active binding site (Sathishkumar *et al*., 2012). Additionally, Bcl-2 active site is built from eight α helix types of polypeptide where ARG66 amino acid residue is the crucial active site residue to activate the inhibition of Bcl-2 (Petros *et al*., 2004; Porter *et al*., 2009). The *in-silico* results showed that both the mangiferin and propafenone possessed a good binding score with mangiferin having a lower binding affinity by -1.0 kcal/mol difference. The superimposed 3D diagram shown in Figure No. 4 (C) revealed mangiferin bound inside the active site together with navitoclax indicating mangiferin is a competitive inhibitor. Binding in the active site, mangiferin and navitoclax shared 10 amino acid residues together, namely ARG66, SER64, LYS22, ARG26, VAL118, VAL115, SER75, ASP62, VAL107, TYR161 and PHE63. Furthermore, hydrophobic interactions were found to dominate to stabilize the ligand-receptor complex were due to hydrophobic amino acids, namely GLY, ALA, VAL, LEU, PHE and MET in the binding site (Pace *et al*., 2012; Sato *et al*., 2018). Mangiferin binds in the active site interacting with ARG66 residue contributes to its good binding score and inhibits Bcl-2. Both mangiferin and propafenone structures mainly contain cycloalkene and aromatics backbone which act as hydrophobes towards hydrophobic amino acids resulted in repelling with each other and stabilize the complex (Barnoud *et al*., 2014; Brylinski, 2018). In addition, the mangiferin and propafenone hydroxyl groups contribute another six and one hydrogen bond respectively to hydrophilic amino acid (ARG, SER) help in stabilizing the binding complex. Bcl-2 protein inhibition causes the imbalance of pro-apoptotic protein Bax and Bak to overexpress and results in apoptosis cascade activation (Hata *et al*., 2015; Kale *et al*., 2018). Second protein, namely Cyclin B/CDK1 complex, another protein that is involved in G2 phase cell cycle arrest. The cyclin B/CDK1 complex consists of 1184 amino acid residues making three chains of A, B and C (Petri *et al*., 2007). The protein structure consists of the N-terminal lobe of the anti-parallel β-sheet connected to the C-terminal lobe of α-helices, glycine-rich loop, α-C-helix, hinge and activation loop where amino acid residues i.e., LYS33, GLU51, and ARG150 are located in the active binding site (Wood & Endicott, 2018; Wood *et al*., 2019). The results showed that mangiferin and propafenone had a good binding score with a difference of -0.2 kcal/mol binding affinity. Moreover, results showed that mangiferin bound inside the catalytic site together with control alvocidib and interacted with the active amino acid residue, namely LYS33, while propafenone bound inside the allosteric site. Both mangiferin and alvocidib showed shared eight amino acid residues in the active site, namely LEU83, LEU135, PHE80, VAL64, VAL18, MET85, ILE10 and GLY11. Surprisingly, propafenone showed to have 18 hydrophobic interactions and 3 hydrogen bonds with the amino acid residues in the binding site more than the mangiferin. This explained why propafenone had a comparatively similar binding affinity with mangiferin. Additionally, type of amino acids presents in the binding site contributed to the binding score with the hydrophobic amino acids (PRO, ALA, ILE and MET) and neutral amino acids (SER, THR, TYR and GLN) involving in the interaction to stabilize the binding (Pace *et al*., 2012; Sato *et al*., 2018). The binding site environment was an advantage to the ligand's hydrophobic structure. Therefore, it segregates from the binding site residues to stabilize the binding. Any disruption of the cyclin B/CDK1 complex causes the cells to fail to enter M

phase and arrest in G2 phase (Goldstone *et al*., 2001; Brown *et al*., 2015).

The third protein responsible for angiogenesis in *Homo sapiens* vascular endothelial growth factors (VEGF) is homodimeric structure which consists of 214 amino acid residues with two chains twisted antiparallel β-sheet, namely V and W (Wiesmann *et al*., 1997). It was also mentioned that each chain consists of β1, β2, β3, β5, β6, α1 and α2 with α1 overlapping with the opposite chain. The active site residues involved in the catalytic events, namely CYS57, GLY59 and LEU32 are located in chain V between β2, β6 and α2 (Chandrasekaran *et al*., 2007; Saha *et al*., 2013). The finding on the docking analysis of VEGF protein revealed that propafenone and mangiferin bound in the active site, while control docking squalene bound in allosteric site suggesting that both ligands were competitive inhibitor and had hydrophobic interaction with the active site amino acid residue, namely GLY59. Mangiferin and propafenone shared similar amino acid residues at binding site viz. SER50, CYS61, CYS51, CYS60, GLU67 and LYS107, therefore explained the comparable binding affinity with a difference of - 0.1 kcal/mol. Besides, the polar amino acids (SER, and CYS) and hydrophobic amino acids, namely LEU, PHE, ILE and GLY, contributed to the hydrophobic interactions by segregating from the water in the surrounding. In addition, the structure of the compounds which are hydrophobic due to the high number of carbons, presence of hydroxyl groups contributed during the binding interaction forming 11 hydrophobic interactions with the amino acid residues and additional two and four hydrogen bonds for mangiferin and propafenone, respectively. The inhibition of VEGF protein will disrupt the development of new capillaries from the pre-existing vascular network. The VEGF protein plays a pivotal role in the development of new capillaries from the pre-existing vascular network. Hence, inhibition of activating VEGFR-1 and VEGFR-2 resulted in inhibition of angiogenesis cascade, proliferation, migration and survival in endothelial cells (Tahergorabi & Khazaei, 2012).

Nucleoside diphosphate kinase (NM23-H1) responsible for suppressing metastasis is a hexamer with the asymmetric unit build up from 456 amino acid residues and the structure is composed of two trimers on top of each other with subunits labelled A, B, C in a trimer and D, E, F in another trimer (Morera *et al*., 1995). The subunits are identical folded into a compact of α/β domain followed by C-terminal extension in antiparallel structure. The protein active sites are positioned in chain C with PHE60, VAL112, ASP54, ARG88 amino acid residues building the catalytic pocket (Postel *et al*., 2002). The 3D superimposed diagram of the receptor-ligand complex for NM23-H1 protein in Figure No. 7C indicates mangiferin and propafenone shared catalytic site, which showed both ligands were non-competitive activator to NM23-H1. Furthermore, the ligand interacts with the same residues which are LEU64, VAL112, LYS12, ASN115, GLY113, GLY63, LEU64, LEU55 and PHE60 during the catalytic event. Both ligands interacted with crucial active site amino acid residues, namely PHE 60 and VAL112 to activate NM23-H1 protein (Dexheimer *et al*., 2009). The analysis on residues involved showed hydrophobic interactions dominated to stabilize the protein structure during the catalytic event. Hydrophobic and polar amino acids (VAL, LEU, PHE, TYR, and GLN) interacted with the hydrophobic molecules in ligands, therefore, resulted in hydrophobic interaction (Blaha-Nelson *et al*., 2017). Furthermore, a significant number of hydrogen bonds formed in the catalytic event for all ligands with amino acid residues (LYS, ASN, ARG) due to hydroxyl and carboxyl functional groups interaction which was aided by the presence of water molecules in the protein (Zhao & Huang, 2011). NM23-H1 protein overexpression predicts a favourable prognosis for melanoma patients (Bunce & Khanim, 2018). Hence, activating NM23-H1 promotes its metastatic suppression potential, including inhibiting cancer motility, invasion, and colonization (Prabhu *et al*., 2012).

The molecular docking analysis demonstrated the highest binding affinity viz. -8.2 kcal/mol by mangiferin on Bcl-2 protein and propafenone on cyclin B/CDK1 complex. Additionally, cyclin B/CDK1 complex protein showed as the most favourable for binding as both ligands had a high binding score with -8.2 and -8.0 kcal/mol for propafenone and mangiferin, respectively compared to other proteins. Mangiferin in this study demonstrated that it was found to bound in the active site for all the four proteins while propafenone was found to bound in allosteric site for Bcl-2 and cyclin B/CDK1 complex, however bound in the active sites for VEGF and NM23-H1 proteins. The present study

showed that hydrophobic interactions were dominant and assisted the catalytic events due to mangiferin and propafenone carbon structure backbone which acted as hydrophobes. Moreover, this study demonstrated anticancer effects of mangiferin and propafenone individually evidenced through an *in silico* data on four different anticancer target proteins. This result might support future studies to further confirm a possibility that both compounds might act synergistically in exhibiting better anticancer effect.

CONCLUSION

The *H. brachyura* phytobezoar is a rare material which makes it unsustainable for commercialization and bioactive compounds isolation. Therefore, LC-MS-based metabolomics analysis is an appropriate technique in investigating the possible bioactive compounds of *H. brachyura* bezoar possessing anticancer activity. Methanol extract exhibited the highest cytotoxicity activity compared to other extracts. Two putative active compounds were identified from the methanol *H. brachyura* bezoar extract using a multivariate data analysis approach by correlating LCMS with the cytotoxicity activity on A375 cells. The compounds identified, namely mangiferin and propafenone, are reported for the first time to present in the *H. brachyura* bezoar through this study. The molecular docking study predicted the binding mode and binding interactions between the identified compounds and the proteins, namely Bcl-2, cyclin B/CDK1 complex, VEGF and NM23-H1. The finding suggested that mangiferin and propafenone have the potential to act as an anticancer agent by inducing apoptosis, arrest cells in G2 phase, inhibit angiogenesis and metastasis. Hence, mangiferin and propafenone can be further explored to develop novel anticancer agents in the future studies.

ACKNOWLEDGMENTS

Authors would also like to acknowledge the Ministry of Higher Education (MOHE), Malaysia for funding this research through FRGS 16-045-0544 and Department of Wildlife and National Parks Malaysia for granting permission to perform this study.

Continuation of author affiliations:

[6]Institute of Biological Sciences, Faculty of Science, University of Malaya, Kuala Lumpur, Malaysia

[7]Center for Research in Biotechnology for Agriculture, Faculty of Science, University of Malaya, Kuala Lumpur, Malaysia

[8]Borneo Research on Algesia, Inflammation and Neurodegeneration (BRAIN) Group, Faculty of Medicines and Health Sciences, University Malaysia Sabah, Kota Kinabalu, Sabah, Malaysia

[9]Department of Preclinical, International Medical School, Management and Science University, Shah Alam, Malaysia

REFERENCES

Ahmad N, Nasir SM, Amin A. 2012. Perceptions on captive Malayan Porcupine (*Hystrix brachyura*) meat by Malaysian urban consumers. **Health Environm J** 3: 67 - 78.

Balik M, Kolnikova I, Maly M, Waldauf P, Tavazzi G, Kristof J. 2017. Propafenone for supraventricular arrhythmias in septic shock-comparison to amiodarone and metoprolol. **J Crit Care** 41: 16 - 23. **https://doi.org/10.1016/j.jcrc.2017.04.027**

Barnoud J, Rossi G, Marrink SJ, Monticelli L. 2014. Hydrophobic compounds reshape membrane domains. **Plos Comput Biol** 10. **https://doi.org/10.1371/journal.pcbi.1003873**

Blaha-Nelson D, Krüger DM, Szeler K, Ben-David M, Kamerlin SCL. 2017. Active site hydrophobicity and the convergent evolution of paraoxonase activity in structurally divergent enzymes: The case of serum paraoxonase 1. **J Am Chem Soc** 139: 1155 - 1167. **https://doi.org/10.1021/jacs.6b10801**

Bray F, Ferlay J, Siegel ISRL, Torre LA, Jemal A. 2018. Global cancer statistics 2018: GLOBOCAN estimates of incidence and mortality worldwide for 36 cancers in 185 countries. **CA Cancer J Clin** 68: 394 - 424. **https://doi.org/10.3322/caac.21492**

Brown NR, Korolchuk S, Martin MP, Stanley WA, Moukhametzianov R, Noble MEM, Edicott JA. 2015. CDK1 structures reveal conserved and unique features of the essential cell cycle CDK. **Nature Commun** 6: 1 - 12. **https://doi.org/10.1038/ncomms7769**

Brylinski M. 2018. Aromatic interactions at the ligand-protein interface: Implications for the development of docking scoring functions. **Chem Biol Drug Design** 91: 380 - 390. **https://doi.org/10.1111/cbdd.13084**

Bunce CM, Khanim FL. 2018. The "known-knowns", and "known-unknowns" of extracellular Nm23-H1/NDPK proteins. **Lab Invest** 98: 602 - 608. **https://doi.org/10.1038/s41374-017-0012-5**

Chandrasekaran V, Ambati J, Ambati BK, Taylor EW. 2007. Molecular docking and analysis of interactions between vascular endothelial growth factor (VEGF) and SPARC protein. **J Mol Graph Model** 26: 775 - 782. **https://doi.org/10.1016/j.jmgm.2007.05.001**

Chung YF, Lim NTL, Shunari M, Wang D, Chan SKL. 2016. Records of the Malayan porcupine, *Hystrix brachyura* (Mammalia: Rodentia: Hystricidae) in Singapore. **Nature in Singapore** 9: 63 - 68.

Coxon CR, Anscombe E, Harnor SJ, Martin MP, Carbain B, Golding BT, Hardcastle IR, Harlow LK, Korolchuk S, Matheson CJ, Newell DR, Noble MEM, Sivaprakasam M, Tudhope SJ, Turner DM, Wang LZ, Wedge SR, Wong C, Griffin RJ, Endicott JA, Cano C. 2017. Cyclin-dependent kinase (CDK) inhibitors: Structure - activity relationships and insights into The CDK - 2 selectivity of 6 - substituted 2 - arylaminopurines. **J Med Chem** 60: 1746 - 1767. **https://doi.org/10.1021/acs.jmedchem.6b01254**

Dexheimer TS, Carey SS, Zuohe S, Gokhale VM, Hu X, Murata LB, Maes EM, Weichsel A, Sun D, Meuillet EJ, Montfort WR, Hurley LH. 2009. NM23-H2 may play an indirect role in transcriptional activation of C-Myc gene expression but does not cleave the nuclease hypersensitive element III 1. **Mol Cancer Ther** 8: 1363 - 1377. **https://doi.org/10.1158/1535-7163.MCT-08-1093**

Du S, Liu H, Lei T, Xie X, Wang H, He X, Tong R, Wang Y. 2018. Mangiferin: An effective therapeutic agent against several disorders (Review). **Mol Med Rep** 18: 4775 - 4786. **https://doi.org/10.3892/mmr.2018.9529**

Eriksson L, Byrne T, Johansson E, Trygg J, Vikström C. 2013. **Multi- and megavariate data analysis: Basic principles and application**. Third, Umea, Sweden.

Firus Khan AY, Ahmed QU, Narayanamurthy V, Razali S, Asuhaimi FA, Saleh MSM, Johan MF, Khatib A, Seeni A, Wahab RA. 2019a. Anticancer activity of Grassy *Hystrix brachyura* Bezoar and its mechanisms of action: An *in vitro* and *in vivo* based study. **Biomed Pharmacother** 114: 108841. **https://doi.org/10.1016/j.biopha.2019.108841**

Firus Khan AY, Asuhaimi FA, Jalal TK, Roheem FO, Natto HA, Johan MF, Ahmed QU, Wahab RA. 2019b. *Hystrix brachyura* Bezoar characterization, antioxidant activity screening, and anticancer activity on melanoma cells (A375): A preliminary study. **Antioxidants** 8: 1 - 15. **https://doi.org/10.3390/antiox8020039**

Firus Khan AY, Ahmed QU, Nippun TS, Hilles A, Jalal TK, Teh LK, Salleh MZ, Noor SM, Seeni A, Khatib A, Wahab RA. 2020. Determination toxic effects of *Hystrix brachyura* Bezoar extracts using cancer cell lines and embryo Zebrafish (*Danio rerio*) models and identification of active principles through GC-MS analysis. **J Ethnopharmacol** 262: 1 - 13. **https://doi.org/10.1016/j.jep.2020.113138**

Ghagane SC, Puranik SI, Kumbar VM, Nerli RB, Jalalpure SS, Hiremath MB, Neelagund S, Aladakatti R. 2017. *In vitro* antioxidant and anticancer activity of *Leea indica* leaf extracts on human prostate cancer cell lines. **Integ Med Res** 6: 79 - 87. **https://doi.org/10.1016/j.imr.2017.01.004**

Gold-Smith F, Fernandez A, Bishop K. 2016. Mangiferin and cancer: Mechanisms of action. **Nutrients** 8: 16 - 20. **https://doi.org/10.3390/nu8070396**

Goldstone S, Pavey S, Forrest A, Sinnamon J, Gabrielli B. 2001. Cdc25-dependent activation of cyclin A/Cdk2 is blocked in G2 phase arrested cells independently of ATM/ATR. **Oncogene** 20: 921 - 932. **https://doi.org/10.1038/sj.onc.1204177**

Ha S, Choi J, Min NAY, Lee K, Ham SW. 2017. Inhibition of importin B1 with a 2-aminothiazole derivative resulted in G 2 / M cell-cycle arrest and apoptosis. **Anticancer Res** 37: 2373 - 2379. **https://doi.org/10.21873/anticanres.11575**

Hanahan D, Weinberg R. 2000. The hallmarks of cancer review University of California at San Francisco. **Cell** 100: 57 - 70. **https://doi.org/10.1016/s0092-8674(00)81683-9**

Hanahan D, Weinberg RA. 2011. Hallmarks of cancer: The next generation. **Cell** 144: 646 - 674. **https://doi.org/10.1016/j.cell.2011.02.013**

Hata AN, Engelman JA, Faber AC. 2015. The BCL2 family: Key mediators of the apoptotic response to targeted anticancer therapeutics. **Cancer Discov** 5: 475 - 487. **https://doi.org/10.1158/2159-8290.CD-15-0011**

Kale J, Osterlund EJ, Andrews DW. 2018. BCL-2 family proteins: Changing partners in the dance towards death. **Cell Death Differ** 25: 65 - 80. **https://doi.org/10.1038/cdd.2017.186**

Khan I, Steeg PS. 2018. The Relationship of NM23 (NME) metastasis suppressor histidine phosphorylation to its nucleoside diphosphate kinase, histidine protein kinase and motility suppression activities. **Oncotarget** 9: 10185 - 10202. **https://doi.org/10.18632/oncotarget.23796**

Khurana RK, Kaur R, Lohan S, Singh KK, Singh B. 2016. Mangiferin: A promising anticancer bioactive. **Pharmaceut Patent Anal** 5: 169 - 181.

Li H, Huang J, Yang B, Xiang T, Yin X, Peng W, Cheng W, Wan J, Luo F, Li H, Ren G. 2013. Mangiferin exerts antitumor activity in breast cancer cells by regulating matrix metalloproteinases, epithelial to mesenchymal transition, and B-catenin signaling pathway. **Toxicol Appl Pharmacol** 272: 180 - 190. **https://doi.org/10.1016/j.taap.2013.05.011**

Liu Y, Kang X, Niu G, He S, Zhang T, Bai Y, Li Y, Hao H, Chen C, Shou Z, Li B. 2019. Shikonin induces apoptosis and prosurvival autophagy in human melanoma A375 cells via ROS-mediated ER stress and P38 pathways. **Artificial Cells Nanomed Biotechnol** 47: 626 - 635. **https://doi.org/10.1080/21691401.2019.1575229**

Loizzi V, Vecchio V, Gargano G, Liso M, Kardashi A, Naglieri E, Resta L, Cicinelli E, Cormio G. 2017. Biological pathways involved in tumor angiogenesis and bevacizumab based anti-angiogenic Therapy with Special References to Ovarian Cancer. **Int J Mol Sci** 18: 1967. **https://doi.org/10.3390/ijms18091967.1–11**

López-Perea P, Guzmán-Ortiz FA, Román-Gutiérrez AD, Castro-Rosas J, Gómez-Aldapa CA, Rodríguez-Marín ML, Falfan-Cortes RN, González-Olivares LG, Torruco-Uco JG. 2019. Bioactive compounds and antioxidant activity of wheat Bran and Barley husk in the extracts with different polarity. **Int J Food Prop** 22: 646 - 658. **https://doi.org/10.1080/10942912.2019.1600543**

Lunde D, Aplin K, Molur S. 2008. *Hystrix brachyura*. **The IUCN Red List of Threatened Species 2008**: e.T10749A3212358. **https://doi.org/10.2305/IUCN.UK.2008.RLTS.T10749A3212358.en**

Lutfiya AS, Priya S, Manzoor MAP, Hemalatha S. 2019. Molecular docking and interactions between vascular endothelial growth factor (VEGF) receptors and phytochemicals: An *in-silico* study. **Biocatal Agric Biotechnol** 22: 101424.

Morera S, Lacombe M, Yingwu X, Lebras G, Janin J. 1995. X-ray structure of human nucleoside diphosphate kinase B complexed with GDP at 2 A resolution. **Structure** 3: 1307 - 1314. **https://doi.org/10.1016/s0969-2126(01)00268-4**

Nalbantoglu S. 2016. **Metabolomics: Basic principles and strategies.** In Molecular medicine, Eds. Nalbantoglu S, Amri H. Intechopen.

Nipun TS, Khatib A, Ibrahim Z, Ahmed QU, Redzwan IE, Saiman MZ, Supandi F, Primaharinastiti R, El-Seedi HR. 2020. Characterization of A-glucosidase inhibitors from *Psychotria malayana* Jack leaves extract using LC-MS-based multivariate data analysis and *in-silico* molecular docking. **Molecules** 25: 1 - 17. **https://doi.org/10.3390/molecules25245885**

Pace CN, Fu H, Fryar KL, Landua J, Trevino SR, Shirley BA, Hendricks MN, Iimura S, Gajiwala K, Scholtz JM, Grimsley GR. 2012. Contribution of hydrophobic interactions to protein stability. **J Mol Biol** 408: 514 - 528. **https://doi.org/10.1016/j.jmb.2011.02.053**

Pandey AK, Singhi EK, Arroyo JP, Ikizler TA, Gould ER, Brown J, Beckman JA, Harrison DG, Moslehi J. 2018. Mechanisms of VEGF (Vascular Endothelial Growth Factor) inhibitor-associated hypertension and vascular disease. **Hypertension** 71: E1 - E8. **https://doi.org/10.1161/HYPERTENSIONAHA.117.10271**

Peng NY, Wai LL, Yau YL. 2018. Antioxidant and intracellular reactive oxygen species/reactive nitrogen species scavenging activities of three porcupine bezoars from *Hystrix brachyura*. **Pharmacogn Res** 10: 24 - 30. **https://doi.org/10.4103/pr.pr_145_16**

Petri ET, Errico A, Escobedo L, Hunt T, Basavappa R. 2007. The crystal structure of human cyclin B. **Cell Cycle** 6: 1342 - 1349. **https://doi.org/10.4161/cc.6.11.4297**

Petros AM, Olejniczak ET, Fesik SW. 2004. Structural biology of the Bcl-2 family of proteins. **Biochim Biophys Acta Mol Cell Res** 1644: 83 - 94. **https://doi.org/10.1016/j.bbamcr.2003.08.012**

Porter J, Payne A, De Candole B, Ford D, Hutchinson B, Trevitt G, Turner J, Edwards C, Watkins C, Whitcombe I, Davis J, Stubberfield C. 2009. Tetrahydroisoquinoline amide substituted phenyl pyrazoles as selective Bcl-2 inhibitors. **Bioorg Med Chem Lett** 19: 230 - 233. **https://doi.org/10.1016/j.bmcl.2008.10.113**

Postel EH, Abramczyk BA, Gursky SK, Xu Y. 2002. Structure-based mutational and functional analysis identify human NM23-H2 as a multifunctional enzyme. **Biochemistry** 41: 6330 - 6337. **https://doi.org/10.1021/bi025606**

Prabhu VV, Siddikuzzaman, Berlin Grace VM, Guruvayoorappan C. 2012. Targeting tumor metastasis by regulating Nm23 gene expression. **Asian Pacific J Cancer Prev** 13: 3539 - 3548. **https://doi.org/10.7314/apjcp.2012.13.8.3539**

Prager GW, Braga S, Bystricky B, Qvortrup C, Criscitiello C, Esin E, Sonke GS, Martínez GA, Frenel JS, Karamouzis M, Strijbos M, Yazici O, Bossi P, Banerjee S, Troiani T, Eniu A, Ciardiello F, Tabernero J, Zielinski CC, Casali PG, Cardoso F, Douillard JY, Jezdic S, McGregor K, Bricalli G, Vyas M, Ilbawi M. 2018. Global cancer control: Responding to the growing burden, rising costs and inequalities in access. **ESMO Open** 3: 1 - 10. **https://doi.org/10.1136/esmoopen-2017-000285**

Saha S, Islam MK, Shilpi JA, Hasan S. 2013. Inhibition of VEGF: A novel mechanism to control angiogenesis by *Withania somnifera*'s key metabolite withaferin A. **In Silico Pharmacol** 1: 1 - 9.

Sathishkumar N, Sathiyamoorthy S, Ramya M, Yang DU, Lee HN, Yang DC. 2012. Molecular docking studies of anti-apoptotic BCL-2, BCL-XL, and MCL-1 proteins with ginsenosides from *Panax ginseng*. **J Enzyme Inhib Med Chem** 27: 685 - 692. **https://doi.org/10.3109/14756366.2011.608663**

Sato T, Sasaki T, Ohnuki J, Umezawa K, Takano M. 2018. Hydrophobic surface enhances electrostatic interaction in water. **Phys Rev Lett** 121: 206002. **https://doi.org/10.1103/PhysRevLett.121.206002**

Schwarz T, Montanari F, Cseke A, Wlcek K, Visvader L, Palme S, Chiba P, Kuchler K, Urban E, Ecker GF. 2016. Subtle structural differences trigger inhibitory activity of propafenone analogues at the two polyspecific ABC transporters: P-Glycoprotein (P-Gp) and breast cancer resistance protein (BCRP). **Chemmedchem** 1380 - 1394. **https://doi.org/10.1002/cmdc.201500592**

Shan C, Chiew T, Ng H, Chun Y, Mun L, Yam F. 2019. A traditional folk medicine in Malaysia: Porcupine Bezoar. **Oriental Pharm Exp Med** 19: 1 - 6. **https://doi.org/10.1007/s13596-019-00370-4**

Stoschitzky K, Stoschitzky G, Lercher P, Brussee H, Lamprecht G, Lindner W. 2016. Propafenone shows class Ic and class II antiarrhythmic effects. **Europace** 18: 568 - 571. **https://doi.org/10.1093/europace/euv195**

Tahergorabi Z, Khazaei M. 2012. A review on Angiogenesis and its assays. **Iranian J Basic Med Sci** 15: 1110 - 1126.

Wiesmann C, Fuh G, Christinger HW, Eigenbrot C, Wells JA, Vos AM. 1997. Resolution of VEGF crystal structure at 1. 7 A in complex with domain 2 of the Flt-1 receptor. **Cell** 91: 695 - 704. **https://doi.org/10.1016/s0092-8674(00)80456-0**

Wood DJ, Endicott JA. 2018. Structural insights into the functional diversity of the CDK-cyclin family. **Open Biol** 8. **https://doi.org/10.1098/Rsob.180112**

Wood DJ, Korolchuk S, Tatum NJ, Wang LZ, Endicott JA, Noble MEM, Martin MP. 2019. Differences in the conformational energy landscape of CDK1 and CDK2 suggest a mechanism for achieving selective CDK inhibition. **Cell Chem Biol** 26: 121 - 130. **https://doi.org/10.1016/j.chembiol.2018.10.015**

Yokdang N, Nordmeier S, Speirs K, Burkin R, Buxton ILO. 2015. Blockade of extracellular NM23 or its endothelial target slows breast cancer growth and metastasis. **Integr Cancer Sci Ther** 2: 192-200. **https://doi.org/10.15761/icst.1000139**

Zhao H, Huang D. 2011. Hydrogen bonding penalty upon ligand binding. **Plos One** 6: 1 - 8. **https://doi.org/10.1371/journal.pone.0019923**

Zheng WB, Li YJ, Wang Y, Yang J, Zheng CC, Huang XH, Li B, He QY. 2017. Propafenone suppresses esophageal cancer proliferation through inducing mitochondrial dysfunction. **Am J Cancer Res** 7: 2245 - 2256.